Analysis of the Equiangular Spiral Antenna on a Dielectric Substrate

Michael McFadden, *Student Member, IEEE*, and Waymond R. Scott Jr., *Senior Member, IEEE*

***Abstract*—While the first equiangular spiral antennas were slots cut from a thin conductive sheet, the widespread availability of cheap photoetching fabrication has made it more common for the spiral to be printed on a dielectric substrate. This paper examines the effects of the substrate on the spiral's performance. The finite-difference time-domain (FDTD) technique is used to model the spiral over a range of configurations. The results are used to construct a design graph that shows that the substrate significantly affects the impedance of the antenna. The results also show that the substrate can negatively impact the bore-sight gain and radiation patterns. Measurements from two spirals are used to verify the accuracy of the numerical model.**

***Index Terms*—Broadband antennas, electromagnetic analysis, spiral antennas.**

I. Introduction

In MANY applications, it is desirable that an antenna perform the same way at every frequency. Rumsey summarized the features that an antenna with this property would have [1]. Prior to his work, it had been observed that the impedance and radiation pattern of an antenna vary only with the geometry as described in wavelengths. As a consequence, changing the operating frequency of an antenna is equivalent to scaling its geometry. This is referred to as the scaling principle or principle of similitude. Rumsey suggested that an antenna with a geometry that was invariant to scaling transformations would be frequency independent.

Geometries that satisfy this requirement must be infinitely large. However, finite approximations to these antennas may still have arbitrarily large bandwidths if the finite antenna radiates in the same way as the infinite one. In order to truncate the antenna properly, at any particular frequency, the majority of the radiation from the infinite antenna must be concentrated in a finite region. Rumsey referred to this necessity as the truncation principle.

The class of geometries that are identical after a scaling transformation consists of angular and conic sections such as infinitely large biconical antennas or bowties. Unfortunately, geometries of this type depend on their truncation to radiate effectively, and consequently fail to adhere to Rumsey's truncation principle.

Manuscript received March 30, 2007; revised July 17, 2007. This work was supported in part by the U.S. Army Research Office under Contract DAAD19-02-1-0252 and the U.S. Army Engineer Research and Development Center Near-Surface Phenomenology Program under Contract 912HZ-07-C-0026.

The authors are with the School of Electrical and Computer Engineering, Georgia Institute of Technology, Atlanta, GA 30332-0250 USA (e-mail: m.mcfadden@gatech.edu; waymond.scott@ece.gatech.edu).

Digital Object Identifier 10.1109/TAP.2007.908838

However, slightly less restrictive requirements did lead to some successful frequency-independent antennas. If the requirements placed on the antenna's geometry by the scaling principle are only enforced for certain scaling parameters, the class of log-periodic antennas may be derived [2], [3]. Rumsey proposed an alternative way to relax the requirements which allowed scaling to modify the antenna's geometry, but only by a rotation. This clearly would leave the impedance properties of the antenna the same. If, in addition, the radiation pattern of the antenna were rotationally symmetric, then true frequency independence could be achieved. Rumsey's specifications led to Dyson's development of the equiangular spiral antenna and its generalization, the conical spiral [4], [5]. Over the next 50 years, the spiral was the subject of a number of numerical and analytical studies [2], [6]–[11]. It has been used in various applications including direction finding, ground penetrating radar, and global positioning systems [12]–[14].

This paper will focus exclusively on the planar equiangular spiral operating in free space and examine the impedance, bore-sight gain, and radiation pattern of the antenna. Previous work in this area has primarily focused on the operation of the antenna without a dielectric backing. In his original work, Dyson developed estimates for the usable frequencies of the planar slot-spiral antenna and explored how the truncations affected the radiation pattern but the slot-spiral does not require a substrate. Wentworth and Rao performed a parametric study on the spiral, but they did not include the effects of a dielectric backing [9].

Some effort has been put into determining the effect of a substrate on the impedance of the antenna [15], [16], but to date there has not been the exhaustive study that is best achieved by a full numerical analysis. This effect will be explored in this paper and design graphs showing the antenna's impedance as the dielectric constant and thickness are varied will be provided. In addition, the bore-sight gain and radiation pattern in the presence of the substrate will be discussed and a simple model will be proposed to explain the behavior of the bore-sight gain.

II. Antenna Geometry and Operation

In [1], Rumsey derives a curve that satisfies the property that a scaling is equivalent to a rotation. This curve is written in polar coordinates as $r(\theta) = \exp(a\theta + b)$ where the constant a determines the rate of wrapping and the constant b rotates the curve. The curve, called the equiangular spiral, has the property that at any two points the angles between the tangent and radial vectors are equal. In fact, this angle is frequently used to describe the spiral's geometry instead of a. The angle, here denoted ψ, can be related to a by $\tan(\psi) = 1/a$.

When this curve is repeatedly rotated by 90°, it forms the edges of a two-armed self-complementary structure as shown in

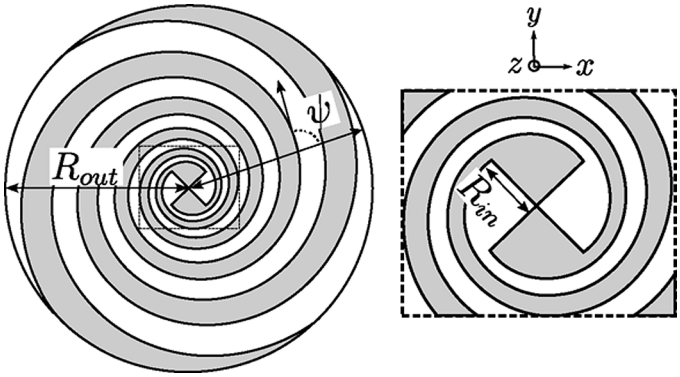

Fig. 1. Geometry of a truncated two-arm equiangular spiral antenna.

Fig. 1. The exterior of the antenna may be truncated in a number of ways. The truncation used in Fig. 1 was introduced by Dyson in [17] because it maximizes the number of turns for a given outer radius.

If the geometry is such that the spiral arms become close enough together to directly connect to a waveguide, no additional feed section is necessary at the inner truncation. However, due to fabrication tolerances, this is often not possible. In this study, a self-complementary bowtie structure is used to feed the antenna.

The spiral has been observed to radiate a circularly polarized wave with approximately constant impedance and gain properties over a wide range of frequencies. Numerical results have shown that the radiation from a particular frequency component f is concentrated in a ring of circumference $\lambda = c/f$ [2]. A simple model is sometimes used to explain this result. The model was first proposed by Kaiser and was initially used to describe the operation of the Archimedean spiral [18], [19]. In the model, the spiral is described as a transmission line structure that transforms into a radiating structure when the traveling wave reaches a ring of circumference $n\lambda$ for integer n.

III. Numerical Modeling

The finite-difference time-domain (FDTD) method is used to model the spirals in this work. A considerable amount of attention has been given to the method in the literature. Interested readers should consult [20] for a full description. As a time-domain method, FDTD allows a wide range of frequencies to be simulated simultaneously by choosing an appropriate excitation. This makes it an excellent choice for modeling a broadband antenna.

In order to calculate the performance of the antenna in free space, the simulation space is truncated with a perfectly matched layer (PML). Radiation patterns are constructed using a near-field-to-far-field transformer (NFFFT). The spiral is inserted as a perfectly conducting 2-D structure by zeroing out the tangential electrical field components interior to the conductor at the end of each component update. The simulation space is divided into sections and each is updated in parallel on a Beowulf cluster using the OpenMPI library.

It is possible to minimize the amount of simulation space in the dimension normal to the spiral plane (the z-axis in Fig. 1) because the structure is essentially 2-D. Since the region very close to the perfect conductor is characterized by extremely sharp drops in the field, a significant amount of evanescent wave content is a concern. The traditional uniaxial PML fails to absorb some evanescent content, therefore the convolutional PML (CPML) proposed by Gedney was implemented instead [21].

In order to verify that the CPML was functioning properly, lower resolution spirals were simulated in large cubic simulation spaces on the order of $500 \times 500 \times 500$ cells. The thickness along the z-dimension was then successively decreased and comparisons were made between impedance and gain calculations for each simulation. In the absence of a dielectric, it was found that the free space surrounding the antenna could be reduced to the point that only four cells lie between the metal surface and the CPML boundary in the z-dimension regardless of the cell size without any significant effect on the measured parameters. This result is in agreement with Gedney's reports on the CPML in [21]. In problems where the spiral's dielectric is included, the simulation space remains fairly thin and the numerical mesh has a typical size of $1000 \times 1000 \times 40$ cells for the spirals run in the design graph section.

Since the PML thickness is ten cells, the volume of the space filled with PML is equal to and in some cases larger than the simulation space itself. In addition, the NFFFT surface contains a comparable number of cells to the simulation space itself. In many simulations, the majority of the computation time is spent on the PML and NFFFT calculations.

The feed of the antenna was implemented by attaching a separate 1-D transmission line simulation into the grid at the center point of the bowtie. The details of this method are described in [22]. This feed allowed the source to be matched to the impedance of the line thereby reducing the length of the required reflection response time when the spiral was excited in frequencies of interest.

IV. Validation by Measurement

Two spirals with design parameters $\psi = 79°$, $R_{\text{in}} = 3$ mm, and $R_{\text{out}} = 0.114$ m were fabricated for measurements to demonstrate the validity of the simulated data. The first was made on Arlon Foamclad R/F 100 with a thickness of approximately 1 mm. Foamclad is a composite dielectric with a thin layer of polyester film $\epsilon_r = 3.2$, on top of a foam layer ($\epsilon_r \approx 1$). For the second, Rogers RO3006 substrate was used with a thickness of 1.27 mm and $\epsilon_r = 6.15 \pm 0.15$.

The impedance and gain measurements of the spirals were obtained using an HP8720D network analyzer. The outer conductors of two lengths of 085 semirigid coax were electrically bound together with conducting tape to form a balanced transmission line. The line was attached at one end to a Picosecond Pulse Labs 5315 balun. At the opposite end, the outer conductor was removed and the inner conductors of the coax were stripped of their dielectric casing.

Since a set of balanced transmission line calibration standards were not available, removable calibration standards were constructed to perform the match-open-short calibration procedure described in [23]. The calibration standards consisted of a small connector piece built from two subminiature B connector contacts and a disk of polycarbonate. A match (100 Ω chip resistor), open, and short (copper disk), as well as the spiral antenna were

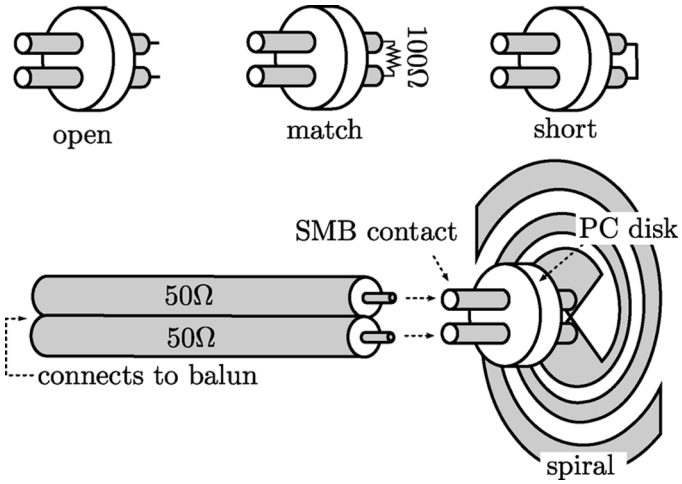

Fig. 2. Calibration standards used in impedance measurement.

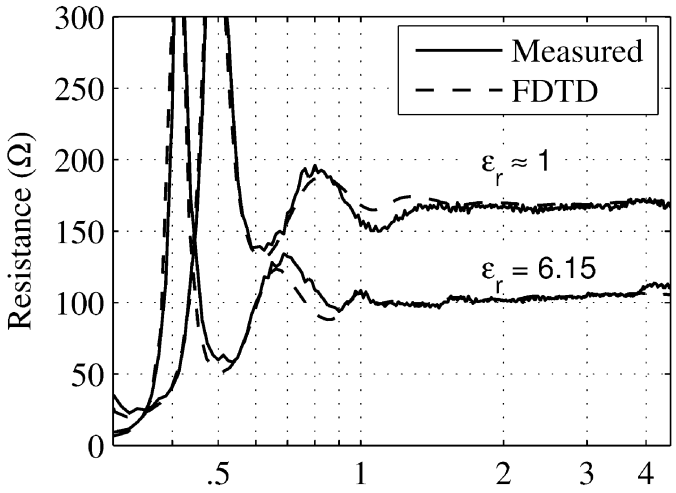

Fig. 3. Comparison of measured and FDTD resistance for the Foamclad and Rogers substrate with design parameters $\psi = 79°$, $R_{\rm in} = 3$ mm, and $R_{\rm out} = 0.114$ m.

soldered to the connector pieces. These calibration standards are shown in Fig. 2.

The two spirals were simulated in the finite-difference model. The Rogers substrate was modeled as a uniform dielectric with $\epsilon_r = 6.15$. The Foamclad substrate was modeled as a 0.1-mm layer of polyester and the foam layer was approximated with air. Comparisons between the measured and simulated impedances for the Foamclad and Rogers spirals are shown in Figs. 3 and 4. The experimental and simulated data show very good agreement. It should also be noted that the resistance of the Foamclad spiral is near 188 Ω as expected.

Bore-sight gain measurements were also taken for the two spirals. These were performed using the two-antenna method [24]. In order to perform these measurements, the antenna was placed on a table made of low dielectric constant foam 1 m from any scatterers. The gain measurements were time-gated to remove reflections from objects in the test area. The measured and simulated curves for the bore-sight gain of the two spirals are shown in Figs. 5 and 6.

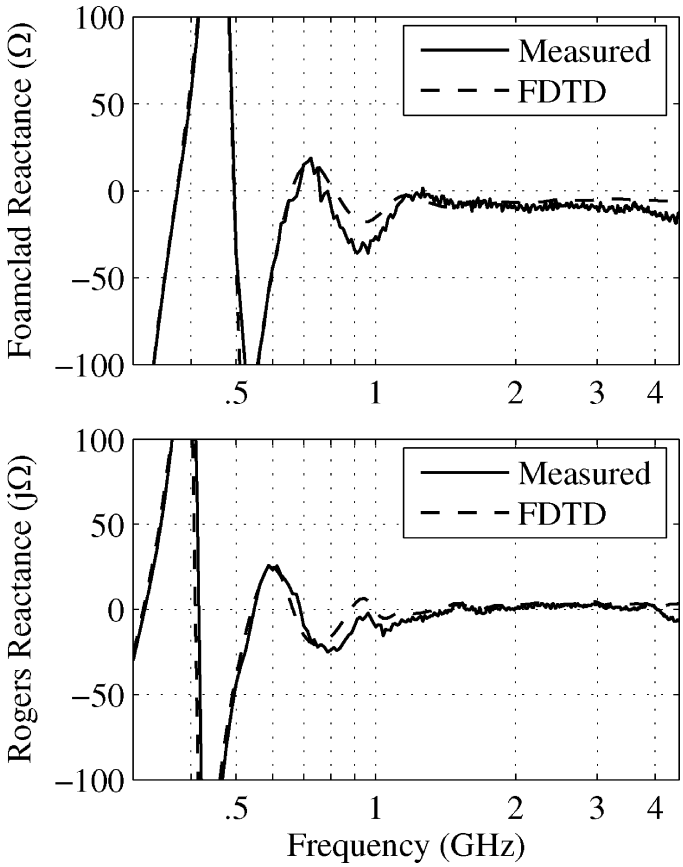

Fig. 4. Comparison of measured and FDTD reactance for the Foamclad and Rogers substrate with design parameters $\psi = 79°$, $R_{\rm in} = 3$ mm, and $R_{\rm out} = 0.114$ m.

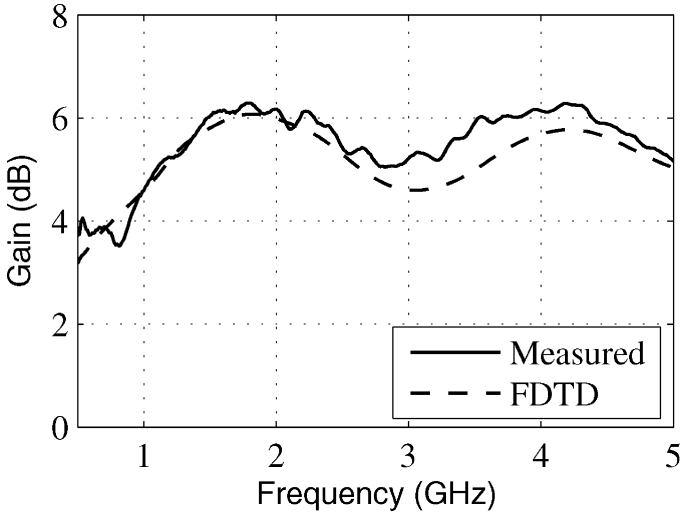

Fig. 5. Comparison of measured and FDTD gain results for the Foamclad substrate with design parameters $\psi = 79°$, $R_{\rm in} = 3$ mm, and $R_{\rm out} = 0.114$ m.

V. Impedance

With the veracity of the numerical results established, several graphs were constructed from simulation data in order to present the effect of the dielectric on the impedance of the spiral antenna. In this section, the theoretical value for the impedance of the spiral is discussed and a plot of the impedance as a function of the most important parameters is provided.

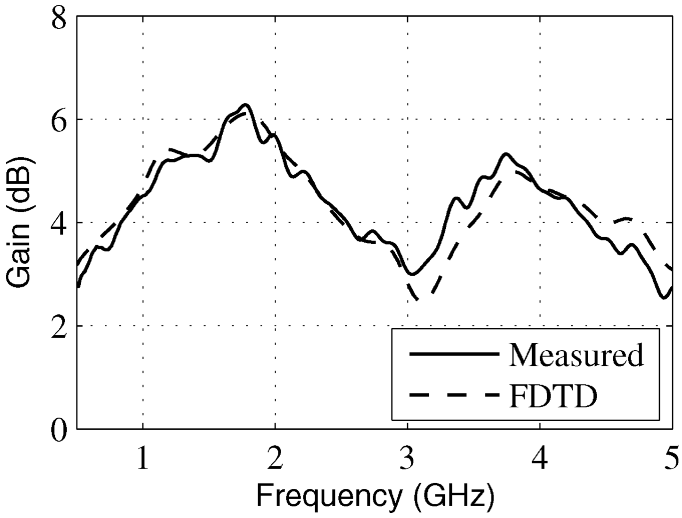

Fig. 6. Comparison of measured and FDTD gain results for the Rogers substrate with design parameters $\psi = 79°$, $R_{\rm in} = 3$ mm, and $R_{\rm out} = 0.114$ m.

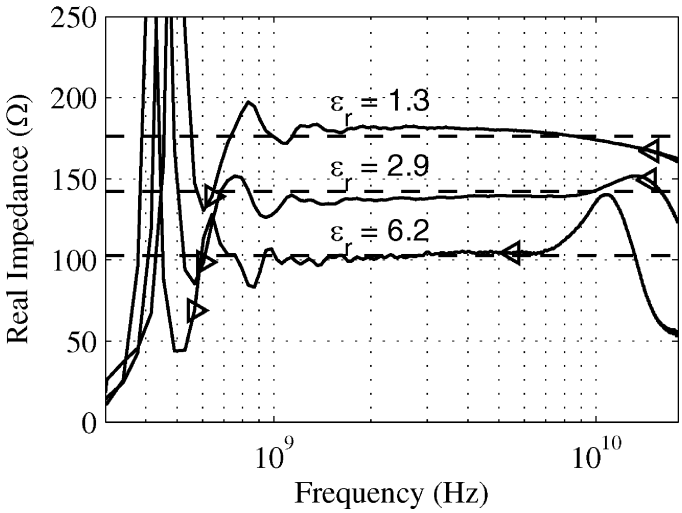

Fig. 7. Real impedance curves for spirals designed to be (top to bottom): 188 Ω, 148 Ω, and 108 Ω. The triangular markers denote the edges of the operating band. The dashed lines show the calculated characteristic impedance, defined here to be the average in the operating band.

A. Impedance Curves

Spiral antenna impedance curves tend to show three distinct regions of behavior. The lower frequencies are dominated by the outer truncation, the upper frequency behavior relates to the inner truncation, and the behavior in the intermediate frequencies is determined by the shape of the spiral curve itself. Portions of the traveling wave model proposed by Kaiser for the Archimedean spiral will be used to explain the form of the curves in a manner similar to [15].

Using the auxiliary 1-D transmission line described in Section III, impedance curves as a function of frequency were calculated for the spiral on the substrates of interest. The real parts of some of these curves are shown in Fig. 7. The imaginary portions are very similar but have an average value of zero regardless of the dielectric.

The spirals used in Fig. 7 had the parameters $\psi = 79°$, $R_{\rm in} = 3$ mm, and $R_{\rm out} = 0.114$ m. Each spiral shown had a 1.27-mm-thick substrate with dielectric constants $\epsilon_r = 1.3$, 2.9, and 6.2 from top to bottom. These values were chosen to progressively decrease the impedance by about 40 Ω. The spiral impedance curves show three important features which are present in all impedance curves seen in this study: The lower frequency region of the impedance is dominated by a series of resonant peaks, the middle frequencies are approximately constant, and the upper frequencies contain either a resonant peak or a region where the real impedance decreases with frequency.

The low-frequency peaks arise from the portion of the energy inserted onto the spiral arms that travels to the end of the spiral and reflects back to the feed without radiating. On an infinitely large spiral, a traveling wave at any particular frequency propagates along the spiral arms until it reaches a circular active region with a circumference equal to one wavelength. At this point, the majority of the energy in the wave is converted to radiation. However, when the spiral is truncated at a given outer radius, all frequencies low enough to have active regions outside the chosen truncation point will reach the edge of the spiral and reflect back to the feed. The reflection causes ripples that take the form of a series of peaks because the current at the feed point consists of the initial feed current I summed with a delayed reflected current $\Gamma I e^{-j\omega t_d}$, where ω is the particular angular frequency of interest, Γ is a reflection coefficient, and t_d is the delay time necessary for the wave to propagate to the end of the spiral arms and back. This sum has a variation which is roughly periodic as a function of frequency. The amplitude of the ripple decreases rapidly as frequency increases and more of the active region for a particular frequency fits onto the antenna. All spirals shown in Fig. 7 will have an outer circumference of one free-space wavelength at 419 MHz. The frequency at which this occurs is typically taken to be the low-frequency cutoff of the spiral.

In the region between the erratic behavior at the upper and lower frequencies, a band of nearly constant impedance is seen. Because this is the expected behavior of a frequency-independent antenna, this region is referred to as the "operating band." Since the spiral arm structure is self-complementary, a spiral lodged in a homogeneous dielectric would have an operating band impedance of

$$Z = \frac{\eta}{2} = \frac{1}{2}\sqrt{\frac{\mu}{\epsilon}} = \frac{1}{2}\sqrt{\frac{\mu_0}{\epsilon_r \epsilon_0}} \tag{1}$$

by Booker's relation [25]. In free space, this impedance is approximately 188 Ω.

In the nonhomogeneous case, the expression may still be used, but the ϵ_r value must be replaced with an equivalent dielectric constant, typically denoted $\epsilon_{\rm EFF}$, which may be thought of as an average of the dielectric constants in the region weighted in some way by the magnitude of the electric field in a given region of space. The value $\epsilon_{\rm EFF}$ is the equivalent homogeneous dielectric constant that would be required to match the phase velocity of the traveling wave on the dielectric backed spiral arms. A wave traveling down the spiral arms will have a different effective permittivity value because the arms become wider with respect to the substrate thickness. In the operating band, the effective permittivity near the inner truncation appears to determine the impedance of the spiral.

When the inner truncation is sufficiently small compared to the substrate thickness, the impedance can be approximated by evaluating Booker's relation in a half-space of dielectric. This approximation and others appear in [15], [16], [26]

$$\epsilon_{\mathrm{EFF}} = \frac{\epsilon_r + 1}{2} \tag{2}$$

$$Z = \frac{\eta_0}{2\sqrt{\epsilon_{\mathrm{EFF}}}}. \tag{3}$$

In Fig. 7, the dashed lines are a computed average value for the operating band impedance and these show a fair agreement with (2) and (3). It may be noted that while the effective permittivity near the feed does predict the operating band impedance with some accuracy, it does not predict the minimum operating frequency very well.

The impedance in the operating band ends with a resonant peak for the thicker, higher dielectric constant substrates, and a downward trend in the impedance otherwise. This upper frequency behavior is caused by the reflection at the discontinuity between the spiral arms and the bowtie structure. The peak may be made more severe by increasing the angle of the bend ψ.

B. Impedance Design Graphs

The impedance of the feed line to the spiral should be matched to the nearly constant value in the operating band seen in Fig. 7. This value is referred to as the characteristic impedance of the spiral Z_c. To obtain this value for a particular spiral's impedance plot $Z(f)$, the interval over which the impedance remained approximately constant was required. This was defined to be the largest interval $[f_{\min}, f_{\max}]$, over which the standard deviation of the impedance in the interval was less than a fixed value. Z_c was then defined as the average value of $Z(f)$ on this interval. The intervals chosen for the curves in Fig. 7 are denoted by the marker arrows and the average values taken are the dashed lines. In this figure and all subsequent figures that make use of the calculation, the maximum standard deviation was set to 7 Ω.

In the description of the spiral in which the conductor thickness is assumed to be zero, five parameters define the spiral. R_{in}, R_{out}, and ψ are defined in Fig. 1. ϵ_r is the dielectric constant of the substrate and h is the thickness of the dielectric substrate. The intention of the design graphs is to relate the characteristic impedance Z_c to these parameters. The graphs should show the function $Z_c(R_{\mathrm{in}}, h, R_{\mathrm{out}}, \psi, \epsilon_r)$ over some restriction of its domain. In the course of this work, it was noted that when the averaging process is taken into account the impedance can be reduced to a function of only two related variables: h/R_{in} and ϵ_r.

Since the average value taken to be the characteristic impedance begins at a frequency high enough to essentially ignore the reflection from the outer truncation, the parameter R_{out} may be neglected as long as the value is large enough to obtain a well-defined operating band. In this study, this was seen to occur when $R_{\mathrm{out}} > 20R_{\mathrm{in}}$. In addition, it was observed that the function Z_c remained approximately constant as the thickness or inner truncation were varied as long as the ratio h/R_{in} remained constant. This can be related to the scaling principle. It was also found through simulations that the parameter ψ has a very minimal effect on the characteristic impedance of the antenna. Instead, ψ changes the impedance plot near the edges of the operating band, leaving the average value the same. This may be seen in Fig. 8 where a spiral's characteristic impedance is evaluated with parameters $R_{\mathrm{out}} = 0.114$ m, $R_{\mathrm{in}} = 3$ mm, $h = 1.27$ mm, and various ϵ_r over a range of ψ.

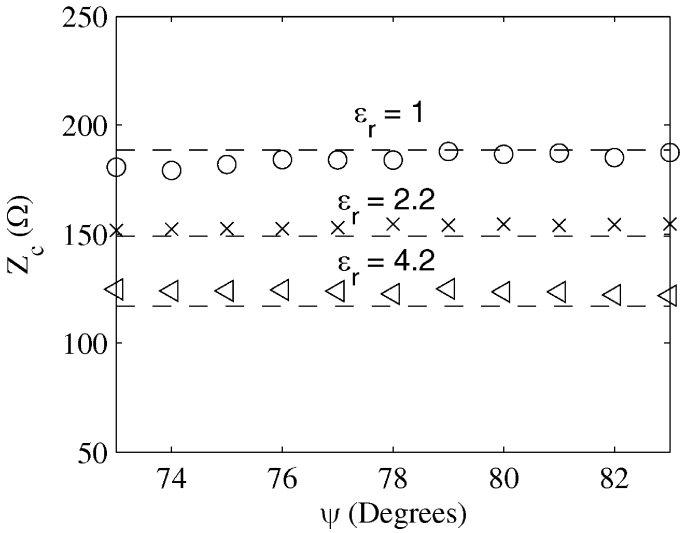

Fig. 8. Z_c as a function of ψ, $R_{\mathrm{out}} = 0.1143$ m, $R_{\mathrm{in}} = 3$ mm, and $h = 1.27$ mm. Dashed values show the impedance estimate in (2) and (3).

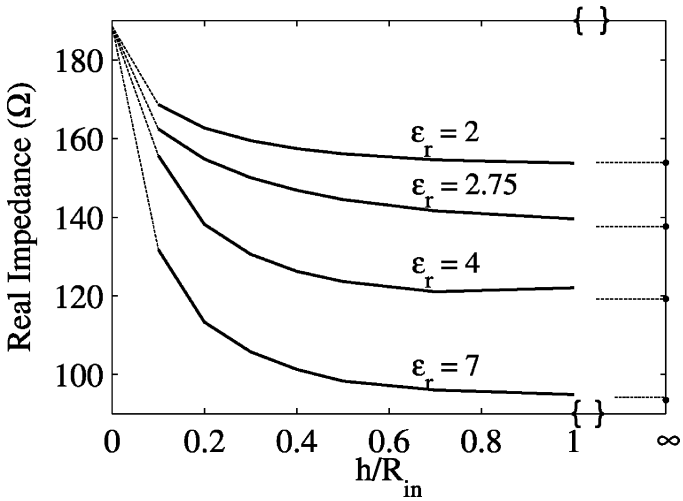

Fig. 9. $Z_c(R_{\mathrm{in}}/h, \epsilon_r)$ with $\psi = 79°$, $R_{\mathrm{in}} = 3$ mm, and $R_{\mathrm{out}} = 0.12$ m. The solid lines are interpolated numerical values. The dashed lines trace the edge of each curve towards its value for no substrate (left) and an infinitely thick substrate (right).

This allows one to define the function $Z_c(h/R_{\mathrm{in}}, \epsilon_r)$ and plot the effect of the substrate on a single graph. The impedance of the spiral was evaluated numerically over the range $0.1 < h/R_{\mathrm{in}} < 1$ for $1 < \epsilon_r < 7$ in Fig. 9. Here, the data was taken from a spiral with a geometry of $\psi = 79°$, $R_{\mathrm{out}} = 0.12$ m, and $R_{\mathrm{in}} = 3$ mm, for various h and ϵ_r.

As seen in Fig. 9, the impedance tends towards the half-space value in (2) and (3) as $h/R_{\mathrm{in}} \to \infty$ and towards the free-space value of $\eta_0/2$ as $h/R_{\mathrm{in}} \to 0$. In the interior region, it is seen that for a moderately thick dielectric ($h/R_{\mathrm{in}} > 0.4$, for instance), the impedance is a strong function of the dielectric constant and a very weak function of the parameter h/R_{in}. Only for a thin

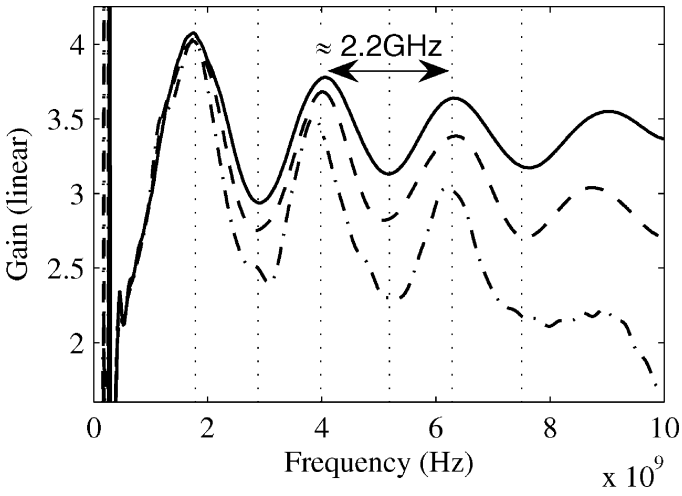

Fig. 10. Simulated gain for a spiral with $\psi = 79°$, $R_{\rm out} = 0.12$ m, and $R_{\rm in} = 2.5$ mm with ϵ_r from highest to lowest: 1, 2.2, and 4.2. Dotted lines denote the minima and maxima of the gain ripple.

dielectric does $h/R_{\rm in}$ show a strong effect on the impedance value.

VI. Gain

The NFFFT was used to determine the radiated field on bore sight for the spiral antenna. The radiated field and simulated impedance were used to derive the directivity of the spiral. Since in this study the conductors are all considered perfect, this value is also the gain on bore sight. Example curves are shown in Fig. 10 for various dielectric constants.

In this section, the behavior of the bore-sight gain as a function of frequency will be examined. The primary effect of the dielectric discussed here will be the tendency of the gain to deteriorate as frequency increases. In addition, the presence of a ripple in the gain plots will be related to the outer truncation of the spiral.

A. Theoretical Bore-Sight Gain on a Substrate

In this section, a simple model of the operation of the spiral is described that shows the same qualitative behavior as the gain curves. Referring to the model proposed by Kaiser and described previously, the energy on the spiral arms can be thought of as a traveling wave on a transmission line. The energy is fed from the center of the line and travels outwards in a spiral path towards an active region where it is radiated away. Since, unlike the Archimedean spiral, the equiangular spiral arms expand, the ratio of the gap width of this transmission line to the height of the substrate becomes smaller as the wave travels along the arms, causing the effective dielectric constant on the line to approach that of free space. Using (3), which appears to describe the impedance of this transmission line at the feed point, one can write the impedance of the transmission line as a function of s, the distance along the line, as

$$Z(s) = \frac{\eta_0}{2\sqrt{\epsilon_{\rm EFF}(s)}} \tag{4}$$

where η_0 is the impedance of free space and $\epsilon_{\rm EFF}(s)$ is the effective permittivity at the location s. While this implies the impedance is always changing along the line, this is an extremely slow variation and it can be assumed that along the ring that constitutes the active region, $Z(s)$ remains constant at some value $Z_{\rm act}$. Since the transmission lines, like the spiral arms, are assumed lossless, the power in the wave remains constant. Therefore, the current in this region remains constant as well.

This then implies that the radiation from the spiral will be that from a traveling ring of current with circumference λ (here, λ is the wavelength of the traveling wave in the active region and is distinguished from the free-space wavelength λ_0). The radiation from a harmonically varying current distribution of angular frequency ω is well known and the details of the integration necessary for a traveling ring of current can be found in [27]. For a ring of circumference λ, one obtains a radiated field

$$E^r(r,\phi,\theta=0,\omega) = e^{-jkr}\frac{\omega\mu_0\lambda I_{\rm act}(\hat{x}-j\hat{y})}{8\pi r} \tag{5}$$

where E^r is the radiated field in phasor form with an assumed $e^{j\omega t}$ time dependence, k is the free-space propagation constant, defined as $k = 2\pi/\lambda_0$, and $I_{\rm act}$ is the magnitude of the traveling ring of current in the active region. Equation (5) shows the expected result that the radiated wave at bore sight is circularly polarized. If the current and impedance at the feed point are denoted $I_{\rm in}$ and $Z_{\rm in}$, respectively, and the effective permittivity in the active region ring is denoted $\epsilon_{\rm act}$, one may use (5) to write the gain G in terms of the known radiated power per unit area on bore sight $P_{\rm rad}(r,\phi,0,\omega)$ and the power inserted into the spiral $P_{\rm in}$

$$P_{\rm rad}(r,\phi,0,\omega) = \frac{|E^r(r,\phi,0,\omega)|^2}{2\eta_0} = \frac{(\omega\mu_0\lambda I_{\rm act})^2}{(8\pi r)^2\eta_0} \tag{6}$$

$$P_{\rm in} = \frac{I_{\rm in}^2 Z_{\rm in}}{2} \tag{7}$$

$$G = 4\pi\frac{P_{\rm rad}}{P_{\rm in}} = \frac{\pi\eta_0 I_{\rm act}^2}{2\epsilon_{\rm act} I_{\rm in}^2 Z_{\rm in}}. \tag{8}$$

Assuming that prior to reaching the ring there was no loss in the traveling wave, one may write

$$\frac{P_{\rm act}}{P_{\rm in}} = 1 \tag{9}$$

$$\Rightarrow \left(\frac{I_{\rm act}}{I_{\rm in}}\right)^2 = \frac{Z_{\rm in}}{Z_{\rm act}} \tag{10}$$

$$G = \frac{\pi}{\sqrt{\epsilon_{\rm act}}} \tag{11}$$

where $P_{\rm act}$ is the power in the wave at the active region and (4) is used in the derivation of (11).

This means that the free-space spiral should radiate a constant gain of π at all frequencies. However, for a spiral on a dielectric substrate, the gain can be expected to monotonically decrease as the frequency increases, moving the active region inward toward the feed. As this occurs, $\epsilon_{\rm act}$ moves upwards towards its value near the feed of approximately $(\epsilon_r + 1)/2$.

Some effort was put into finding a relationship between $\epsilon_{\rm act}$ and the frequency f in order to obtain a functional form for the gain using a transmission line approximation, but aside from the

limiting values discussed previously, the match was unsatisfactory. The effect on the gain is directly related to the failure of the antenna to truly satisfy Rumsey's scaling principle. If the dielectric thickness were to increase as the wave moved outward, the $\epsilon_{\rm act}$ could conceivably be kept constant and this would imply that the gain would remain constant. The data shown in Figs. 5 and 6 show this decreasing behavior with a rate of descent that becomes steeper with a higher dielectric constant. This is again seen in Fig. 10, here with simulated data. In addition to the decreasing gain, a gain ripple is observed with an amplitude of approximately 1 to 2 dB. It will be shown in Section VI-B that this ripple is related to the outer truncation of the spiral.

B. Bore-Sight Gain Ripple

The ripples seen in Figs. 5, 6, and 10 are present in all FDTD simulations of the bore-sight gain in this study as well as measured gain results. In Fig. 10, a sequence of gain curves is shown for various dielectric constants with $\psi = 79°$, $R_{\rm out} = 0.12$ m, and $R_{\rm in} = 2.5$ mm.

Ripples in the frequency domain are often the result of an echo in the time domain, as noted in Section V-A. Here, the radiated field takes the form of some initial pulse $h(t)$ and a delayed scattered pulse $\Gamma h(t - t_d)$. This gives a Fourier transform of the form $\mathcal{F}\{h\}(\omega)(1+e^{-j\omega t_d}\Gamma)$. The magnitude of this function shows a periodic ripple on top of the original response with a period in the frequency domain of $1/t_d$. In Fig. 10, all three plotted gain functions show a ripple with a period of approximately 2.2 GHz which corresponds to a time delay of 0.45 ns. The fact that each of the gain curves shows the same ripple period makes it unlikely that the secondary radiation is the result of the traveling wave in the spiral, since the phase velocity of the traveling wave is a stronger function of the dielectric than the shown variation in the period.

Instead, it would appear that the initial pulse is radiated into free space and the second pulse is the result of some scattering which occurs at a distance of $c(0.45 \times 10^{-9}s) \approx 13.5$ cm. The truncation of the spiral occurs 12 cm from the feed, and after running a number of simulations with various radii for the spirals, it became apparent that the time delay which causes the ripple tends to be approximately R/c, where R is the radius of the spiral. In order to verify that the ripple is related to the truncation of the spiral and to present more convincing support than the theoretical gain model proposed previously, a large spiral was modeled in FDTD so that the secondary ripple could be seen separated from the initial radiated pulse. In Figs. 11 and 12, three spirals with differing dielectric constants and a radius of 1.2 m are shown in the frequency domain and time domain.

The time-domain plots in Fig. 12 show an initial radiation with a peak around 0 ns and a secondary radiation with a peak around 4 ns. The delay is the expected transit time for a spiral of this size. With the two pulses separated, the effect of the secondary radiation can be removed by time gating. This is seen in Fig. 11 as the dotted line. It should be noted that both peaks in the time plot show a chirping property with high frequencies being radiated earlier than low frequencies. This is most easily seen in the $\epsilon_r = 1$ case. The fact that this chirping appears in both pulses suggests that the delayed pulse is a scattering from the radiation in the active region. If the initial pulse

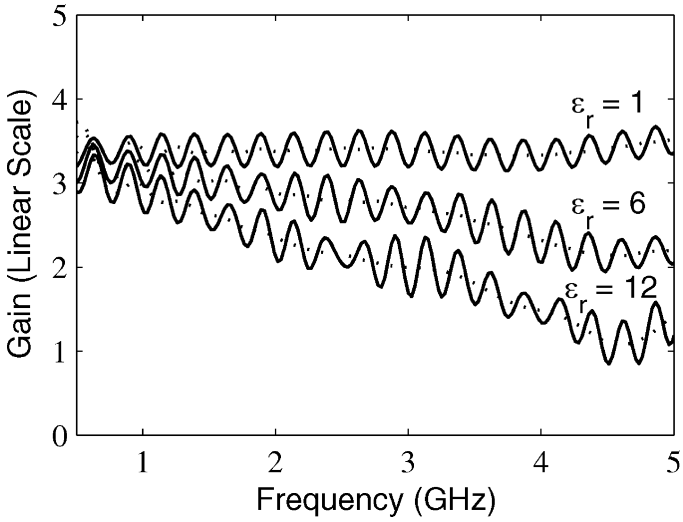

Fig. 11. Simulated gain for three 1.2-m radius spirals (top to bottom): $\epsilon_r = 1$, 6, 11. Time gated gain is shown dotted.

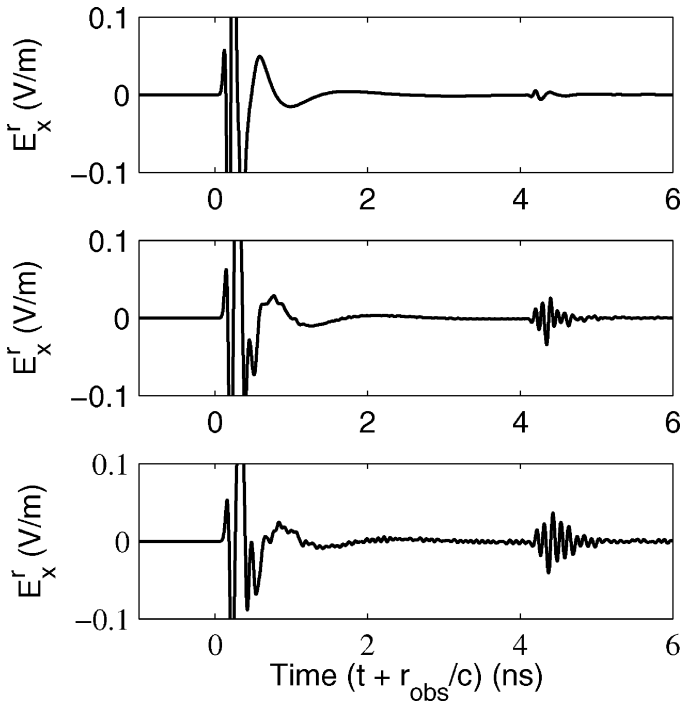

Fig. 12. Time domain response for 1.2-m radius spirals (top to bottom): $\epsilon_r = 1$, 6, 11. Here, $r_{\rm obs}$ refers to the distance from the center of the spiral to an observer in the far field.

were radiated at the feed point then the scattered pulse would be a delayed version of the excitation (a differentiated Gaussian pulse, in this case). Instead, each frequency is believed to be radiated at its active region where $r = \lambda/2\pi$. The signal travels to the outer radius and scatters as depicted in Fig. 13. Since the time delay between the two pulses is $t_d = R/c - v_p/(2\pi fc) = R/c - 1/(\sqrt{\epsilon_{\rm EFF}}\omega)$, the radiated field takes the form

$$\mathcal{F}\{h\}(\omega)(1 + e^{-j\omega t_d}\Gamma) = \mathcal{F}\{h\}(\omega)(1 + e^{-j\omega R/c}e^{-j/\sqrt{\epsilon_{\rm EFF}}}\Gamma) \quad (12)$$

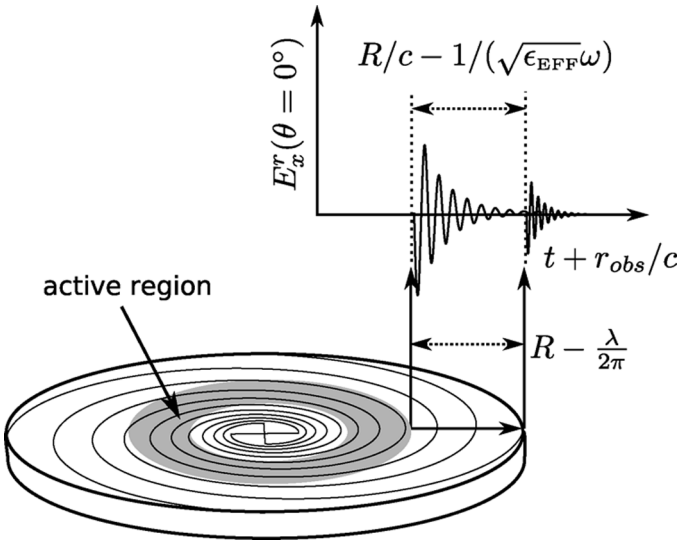

Fig. 13. Diagram of the radiation of a narrowband pulse of angular frequency ω. The time scale shown includes the delay to a far-field observer at $r_{\rm obs}$ from the antenna's center.

which has the periodic variation R/c that is typically observed. It should be noted that this scattering occurs even when the dielectric is not present and only at the outer truncation point of the spiral, not at each successive arm of the spiral that the radiated wave encounters.

C. Radiation Patterns

Since the antenna is modeled as lossless here, the power radiated must still be the power inserted at the feed. Because of this, it may be of interest where the energy that is deflected from bore sight is radiated. This can be determined by constructing a radiation pattern of the antenna. Since the lower hemisphere is almost identical to the upper hemisphere, only the upper hemisphere is shown here. Fig. 14 shows the gain as a function of an angle for the upper hemisphere of the antennas in Fig. 10 at the dielectric constants 4.2 and 1.

In Fig. 14, it can be seen that the scattered pulse acts to alternately expand and contract the pattern along the z-axis in the free-space case. These expansions correspond with the maxima of the gain ripple observed. In the dielectric case, the pattern becomes more complicated at the higher frequencies with more radiated power deflected into sidelobes, but the same behavior is still observed.

The introduction of the absorbing can that is typically used with the spiral antenna could be expected to change the nature of the scattering at the truncation point since there would be an additional scattering off of the can edge. Also, many designers truncate the outer radius of the spiral with absorber to reduce the reflected traveling wave. This may have the added side effect of absorbing the radiated wave described here.

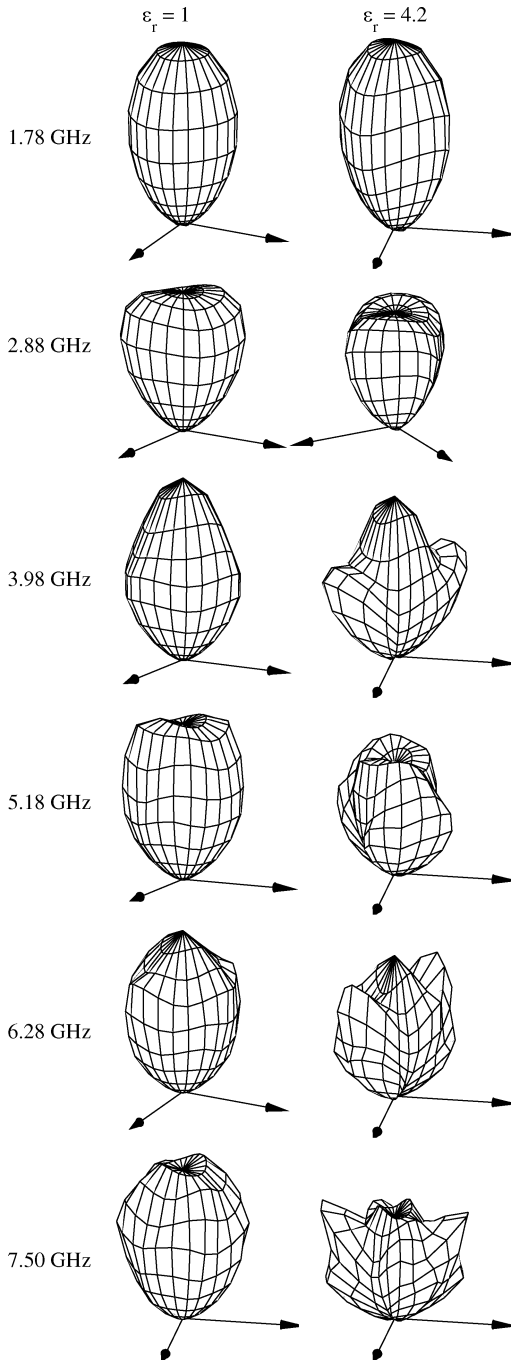

Fig. 14. Radiation patterns for the upper and lower gain curves at the respective minima and maxima denoted in Fig. 10 by dotted vertical lines.

VII. Conclusion

An FDTD model of the spiral element was constructed and compared against measured data. This model was then used to study the effects of the dielectric backing on the spiral. These effects consist of a decrease in the impedance and bore-sight gain over the operating band which becomes more severe as the dielectric constant and substrate thickness are increased. In addition, the source of a scattered radiation that complicates the bore-sight gain as a function of frequency was analyzed. A number of simple models for some of these effects have been presented or summarized from other work. Questions remain as to the nature of the wave that generates the scattered radiation and why it appears to travel radially outward through the spiral arms without scattering, only to scatter at the truncation point.

It is hoped that the design graph presented may be used either as an aid to design or as a conceptual aid. While all results

in this study are for the free-space case, the spiral antenna is typically operated in an absorbing can and preliminary simulations show the impedance graph in Fig. 9 may still be applicable. Some features seen in this study may be specific to the particular method of feeding the antenna with a bowtie and perhaps additional work could show how these effects are changed by different feed methods. In addition, the gain ripple presented in Section VI can be altered by using different types of outer truncations and future work could explore this further as well as determine the effect of the can on the gain ripple observed in the bore-sight gain section.

REFERENCES

[1] V. H. Rumsey, *Frequency Independent Antennas*, H. G. Booker and N. DeClaris, Eds. New York: Academic, 1966, Electrical Science.

[2] R. H. DuHamel and J. P. Scherer, *Antenna Engineering Handbook*, 3rd ed. New York: McGraw-Hill, 1993, ch. 14.

[3] P. E. Mayes, "Frequency-independent antennas and broad-band derivatives thereof," *Proc. IEEE*, vol. 80, no. 1, pp. 103–112, Jan. 1992.

[4] J. D. Dyson, "The equiangular spiral antenna," *IRE Trans. Antennas Propag.*, vol. AP-7, no. 2, pp. 181–187, Apr. 1959.

[5] J. D. Dyson, "The unidirectional equiangular spiral antenna," *IRE Trans. Antennas Propag.*, vol. AP-7, no. 4, pp. 329–334, Oct. 1959.

[6] W. L. Curtis, "Spiral antennas," *IRE Trans. Antennas Propag.*, vol. AP-8, no. 3, pp. 298–306, May 1960.

[7] B. R. Cheo and V. H. Rumsey, "A solution to the frequency-independent antenna problem," *IRE Trans. Antennas Propag.*, vol. AP-9, no. 6, pp. 527–534, Nov. 1961.

[8] Y. S. Yeh and K. K. Mei, "Theory of conical equiangular-spiral antennas, Part I—Numerical technique," *IEEE Trans. Antennas Propag.*, vol. AP-15, no. 5, pp. 634–639, Sep. 1967.

[9] S. M. Wentworth and S. M. Rao, "Analysis of equiangular spiral antennas," *Int. J. Microw. Mill.*, vol. 6, pp. 92–98, 1996.

[10] T. W. Hertel and G. S. Smith, "Analysis and design of two-arm conical spiral antennas," *IEEE Trans. Electromagn. Compat.*, vol. 44, no. 1, pp. 25–37, Feb. 2002.

[11] C. Fumeaux, D. Baumann, and R. Vahldieck, "Finite-volume time-domain analysis of a cavity-backed Archimedean spiral antenna," *IEEE Trans. Antennas Propag.*, vol. 54, no. 3, pp. 844–851, Mar. 2006.

[12] R. G. Corzine and J. A. Mosko, *Four-Arm Spiral Antennas*. Norwood, MA: Artech House, 1990.

[13] N. Padros *et al.*, "Comparative study of high-performance GPS receiving antenna designs," *IEEE Trans. Antennas Propag.*, vol. 45, no. 4, pp. 698–706, Apr. 1997.

[14] W. Clark *et al.*, "The measured effect of soils on ground penetrating radar antenna resolution," in *Proc. 10th Int. Conf. Ground Penetrating Radar*, Delft, The Netherlands, Jun. 2004, pp. 125–128.

[15] W. Weir *et al.*, "Driving-point-impedance measurement and balun design for spiral antennas," Stanford Res. Inst., Menlo Park, CA, Tech. Rep., 1972.

[16] J. A. Huffman and T. Cencich, "Modal impedances of planar, noncomplementary, N-fold symmetric antenna structures," *IEEE Antennas Propag. Mag.*, vol. 47, no. 1, pp. 110–116, Feb. 2005.

[17] J. D. Dyson, "The equiangular spiral antenna," Ph.D. dissertation, Univ. Illinois, Urbana, IL, 1957.

[18] J. A. Kaiser, "The Archimedean two-wire spiral antenna," *IRE Trans. Antennas Propag.*, vol. AP-8, no. 3, pp. 312–323, May 1960.

[19] R. Bawer and J. J. Wolfe, "The spiral antenna," *IRE Trans. Antennas Propag.*, vol. AP-8, no. 1, pp. 84–95, Jan. 1960.

[20] A. Taflove and S. C. Hagness, *Computational Electrodynamics*, 2nd ed. Norwood, MA: Artech House, 2000.

[21] J. A. Roden and S. D. Gedney, "Convolutional PML (CPML): An efficient FDTD implementation of the CFS-PML for arbitrary media," *Microw. Opt. Technol. Lett.*, vol. 27, pp. 334–339, 2000.

[22] J. G. Maloney and G. S. Smith, *Computational Electrodynamics*, 2nd ed. Norwood, MA: Artech House, 2000, ch. 14.

[23] W. Kruppa and K. F. Sodomsky, "An explicit solution for the scattering parameters of a linear two-port measured with an imperfect test set," *IEEE Trans. Microw. Theory Tech.*, vol. MTT-19, no. 1, pp. 122–123, Jan. 1971.

[24] C. A. Balanis, *Antenna Theory*. New York: Wiley, 1982.

[25] H. G. Booker, "Slot aerials and their relation to complementary wire aerials (Babinet's Principle)," *J. Inst. Electr. Eng.*, vol. 93, pp. 620–626, 1946.

[26] T. Iwasaki, A. P. Freundorfer, and K. Iizuka, "A unidirectional semicircle spiral antenna for subsurface radars," *IEEE Trans. Electromagn. Compat.*, vol. 36, no. 1, pp. 1–6, Feb. 1994.

[27] R. S. Elliott, *Antenna Theory and Design*. New York: Wiley-Interscience, 2003.

Michael McFadden (S'04) received the B.S.E.E. and M.S.E.E. degrees from the Georgia Institute of Technology, Atlanta, in 2004 and 2006, respectively, where he is currently working towards the Ph.D. degree.

His research interests include antenna design and numerical modeling.

Waymond R. Scott, Jr. (SM'03) received the B.E.E., M.S.E.E., and Ph.D. degrees from the Georgia Institute of Technology, Atlanta, in 1980, 1982, and 1985, respectively.

In 1986, he joined the School of Electrical and Computer Engineering, the Georgia Institute of Technology, as an Assistant Professor, where he was subsequently promoted to the rank of Professor. His research involves the interaction of electromagnetic and acoustic waves with materials. This research spans a broad range of topics, including the measurement of the properties of materials, experimental and numerical modeling, and systems for the detection of buried objects. Currently, his research is concentrated on investigating techniques for detecting objects buried in the earth.